The pinhole: gateway to ultra-high-resolution three-dimensional radionuclide imaging

Freek Beekman[1, 2], Frans van der Have[1, 2]

[1] Department of Nuclear Medicine, Image Sciences Institute, University Medical Centre Utrecht, Utrecht, The Netherlands
[2] Department of Pharmacology and Anatomy, Rudolf Magnus Institute of Neuroscience, University Medical Centre Utrecht, Utrecht, The Netherlands

Published online: 2 December 2006

Abstract. Today the majority of clinical molecular imaging procedures are carried out with single-photon emitters and gamma cameras, in planar mode and single-photon emission computed tomography (SPECT) mode. Thanks to the development of advanced multi-pinhole collimation technologies, SPECT imaging of small experimental animals is rapidly gaining in popularity. Whereas resolutions in routine clinical SPECT are typically larger than 1 cm (corresponding to >1,000 μl), it has recently proved possible to obtain spatial resolutions of about 0.35 mm (≈0.04 μl) in the mouse. Meanwhile, SPECT systems that promise an even better performance are under construction. The new systems are able to monitor functions in even smaller structures of the mouse than was possible with dedicated small animal positron emission tomography (≈1 mm resolution, corresponding to 1 μl). This paper provides a brief history of image formation with pinholes and explains the principles of pinhole imaging and pinhole tomography and the basics of modern image reconstruction methods required for such systems. Some recently introduced ultra-high-resolution small animal SPECT instruments are discussed and new avenues for improving system performance are explored. This may lead to many completely new biomedical applications. We also demonstrate that clinical SPECT systems with focussing pinhole gamma cameras will be able to produce images with a resolution that may become superior to that of PET for major clinical applications. A design study of a cardiac pinhole SPECT system indicates that the heart can be imaged an order of magnitude faster or with much more detail than is possible with currently used parallel-hole SPECT (e.g. 3–4 mm instead of ≈8 mm system resolution).

Freek Beekman (✉)
Department of Nuclear Medicine,
Image Sciences Institute, University Medical Centre Utrecht,
Utrecht, The Netherlands
e-mail: f.beekman@umcutrecht.nl

Eur J Nucl Med Mol Imaging (2007) 34:151–161
DOI 10.1007/s00259-006-0248-6

Introduction

Today, the majority of clinical procedures using tracers to visualise specific tissue binding sites are carried out with planar gamma camera imaging, single-photon emission computed tomography (SPECT) or positron emission tomography (PET). Imaging of single-photon-emitting radiopharmaceuticals with gamma cameras, in planar or SPECT mode, makes up the largest fraction of these molecular imaging procedures. In addition to clinical SPECT, SPECT imaging with pinholes of experimental animals is currently growing rapidly. The main reason for this is that it allows for both the visualisation and the accurate quantification of molecule concentrations in small animals like rodents with resolutions down to subcompartments of mouse organs. This impacts on most preclinical imaging procedures since rats and mice form the majority of the experimental animal population. The spatial resolution and signal strength of pinhole-collimated gamma cameras are often superior to those with other types of SPECT collimation. The combination of multiple focussing pinhole collimators and advanced software provides even higher resolutions than can be obtained with dedicated small animal PET for many rodent imaging procedures: some novel SPECT systems produce images even at sub-half-millimetre scales. The growing number of experimental small animal models of human physiology and disease will benefit from this development because they require very accurate and non-invasive longitudinal monitoring of molecular dynamics.

Many SPECT tracers are now commercially available that have sufficiently long half-life times to allow for long-distance transportation. Therefore no expensive infrastructure with cyclotrons at site is required. At least eight companies are already manufacturing small animal SPECT devices, with a wide range of pricing and system performance. Many

biomedical research institutes will be equipped with pinhole SPECT in the near future. As a result, non-invasive first-line screening for experimental drugs with radiotracers is expected to become extremely popular.

A primer on the physics of small animal radionuclide imaging (PET and SPECT) was published by King et al. [1], and two overviews of small animal SPECT systems and their place in the matrix of molecular imaging modalities (PET, fluorescence imaging, bioluminescence imaging, magnetic resonance imaging and magnetic resonance spectrometry) were published recently by Meikle et al. [2, 3]. The goal of the present paper is to acquaint a broad readership with the history, physics and mathematics of pinhole SPECT. In addition, we will attempt to place modern pinhole SPECT in the context of past and future SPECT instrumentation and its biomedical applications.

A brief history of pinhole imaging

Since photons travel in straight lines, an inverted image of the illuminated field of view is produced when they pass through a pinhole. The size of the projected image depends on the relative distance between object and pinhole versus pinhole and the surface where the image is projected. This natural phenomenon of pinhole image formation predates the existence of man: For hundreds of millions of years living creatures have existed that have been able to see or sense through holes located in front of a layer of photosensitive tissue such as a retina. A contemporary animal with pinhole eyes is the "living fossil" *Nautilus pompilius* (Fig. 1): it has existed in seas and oceans for about one hundred million years. Another example is the giant clam, which has multiple pinhole eyes; see [4].

We will never know when and how humans first devised pinhole imaging, but situations may have occurred where sun-illuminated scenes were projected upside down through a hole onto the opposite wall of a cave (Fig. 2a). The resulting "movies" may well have astonished primitive man, possibly as long as hundreds of thousands of years ago. What is certain is that several hundreds of years ago, pinhole "cameras" as large as complete living rooms were exploited by artists, for example by Leonardo da Vinci (1452–1519). Da Vinci, and later on artists like Johannes Vermeer (1632–1675), used pinhole projections on the wall of a dark room (Fig. 2b) to trace and draw lines that formed the basis for their paintings and enabled them to obtain an almost perfect perspective. Such devices and their successors are often called "camera obscura" (dark chamber), a term which, according to some historians, was first used by the astronomer Johannes Kepler. Much later, Joseph Nicéphore Niépce built the first pinhole camera with a storage medium (film!) which produced the first photographs. This occurred about a hundred and eighty years ago [5, 6].

In clinical radionuclide imaging, the pinhole has served as a means to collimate gamma rays since the earliest gamma cameras [7–9]. Up until now, the pinhole gamma camera has been used mainly for the imaging of small volumes such as the human thyroid (e.g. [10]). Pinhole imaging involving the use of more than one pinhole simultaneously (multi-pinhole imaging, the nuclear application of which was described as long ago as 1973 [11]) was used to image relatively small organs such as the human thyroid [12], shoulder [13, 14], hip [15, 16], neck [17] and heart [18]. So far, however, multi-pinhole imaging has not achieved broad clinical application. Nevertheless, it can be said that (multi) pinhole-like imaging was "invented" by nature and through the ages has been reinvented over and over again, which applies to many principles of engineering.

Principles of planar radionuclide pinhole imaging

Pinhole imaging with gamma rays is based on the same geometric principle as the optical pinhole camera. A scintillation crystal is used to determine the gamma ray intensity projection: the scintillation light pattern is read out with a position-sensitive light detector, instead of a film. In optical cameras, pinholes have been replaced by lenses, since this allows for more light photons to be captured. Since there are no practical methods for diffracting or reflecting gamma rays for SPECT, today collimators are used for imaging single-photon-emitting radionuclides, although these transmit only a tiny fraction of the gamma quanta emitted by tracers in the animal or patient. Most collimators consist of a radiation-absorbing wall with one or more narrow holes. While for animals pinhole collimators are popular, the parallel-hole collima-

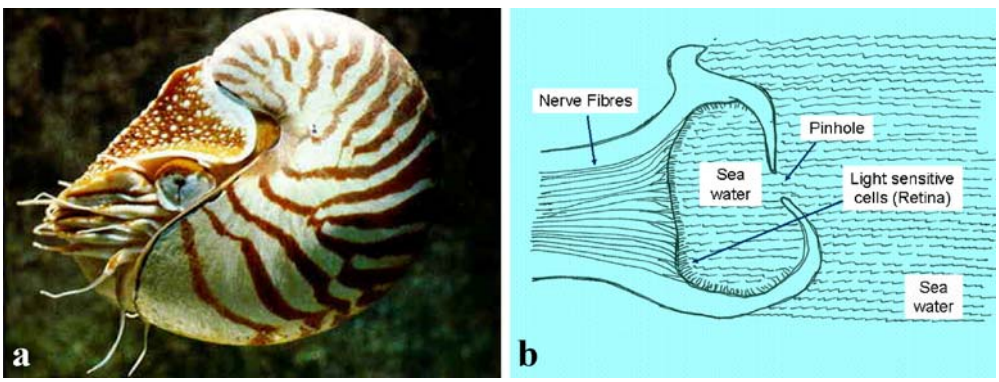

Fig. 1. The *Nautilus pompilius* (**a**, image courtesy of Artis Zoo, Amsterdam) with pinhole eyes (**b**)

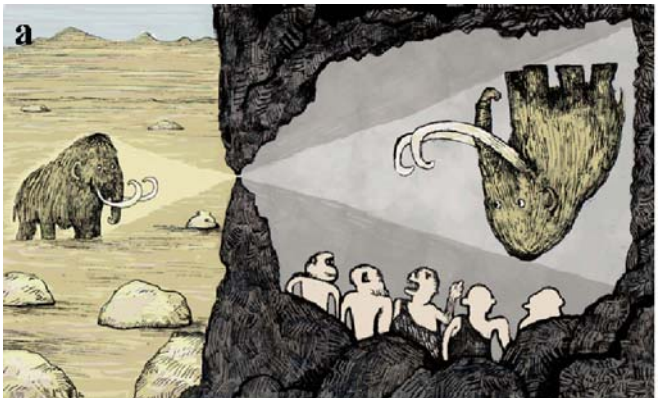

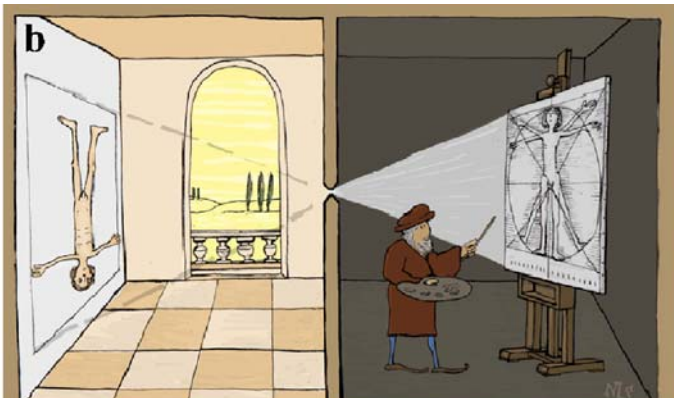

Fig. 2. a An artist's impression of possible early pinhole imaging: the film-less movie theatre was born when surrealistic "upside down movies" were displayed on the wall of a cave. **b** Was this how Leonardo painted the Vitruvian Man? A trade-off between "patient" discomfort and artist discomfort could be found by changing the angular position of the model. Illustrations by Niels de Hoog

tor is the clinical work horse. It consists of a slab of lead with a thickness of a couple of centimetres, with many narrow parallel holes very close to each other (Fig. 3, left). Today, these collimators are relatively easy to produce, and are suitable for imaging large areas of the body. SPECT images can be reconstructed rapidly and simply from parallel-hole projections.

Why do pinhole collimators produce images with a much higher resolution than parallel-hole collimators when used to image small animals or small organs? And why can this resolution be even better than the amount of blurring due to the detector properties themselves (already a few millimetres)? This is explained in Figs. 3 and 4. Figure 3 shows a mouse of size T that is projected through a parallel-hole collimator (left side) and through a pinhole (right side). In the case of an "ideal" parallel-hole collimator, the projection of the object is blurred only by the intrinsic gamma camera resolution. The blurring is caused by: (a) scintillation light that spreads out in the crystal, (b) the limited number of light photons generated per gamma interaction in the crystal, which results in position uncertainty of the detected scintillation light flash, and (c) the limited positioning abilities of the position-sensitive light detector behind the crystal. The intrinsic camera resolution is characterised by a value R_i which describes the width of the blob that appears when a pencil gamma beam is used to irradiate the crystal. For most clinical gamma cameras, R_i is about 3.5 mm full-width at half-maximum (FWHM). With pinholes we have a different situation: when the distance between the mouse and the pinhole is L and that between the pinhole and the detector is $5\times L$, the size of the mouse projection is $5\times T$. Therefore, when the mouse is de-magnified to its original size, it is not smoothed with an amount corresponding to R_i, but is smoothed only with $R_i/5$. The smaller the object, the closer it can be placed to the pinhole without protruding out of the field of view, and therefore the higher the magnification factor and the resolution can be. A pleasant side-effect of using pinholes for small animals is that the fraction of detected photons (the so-called sensitivity, denoted here by S) in the field of view increases spectacularly when the object is closer to the pinhole. This is because the solid angle at which photons from each point in the object are able to pass through the pinhole increases tremendously for points closer to the pinhole. This relationship can be approximated by: $S = D_{eff}^2 \Big/ (16\, z^2)$ where D_{eff} is the effective hole diameter (accounting for penetration of rays through the aperture edges) and z, the object-to-pinhole distance. With parallel holes, the fraction of detected photons from a small source in air is almost independent of the camera distance. Experimental data acquired at Duke University (Fig. 4, from [19]) clearly demonstrate this effect: both sensitivity and resolution obtained with pinholes beat those of a parallel-hole collimator when the object is close to the pinhole opening. Extreme exploitation of this magnification and sensitivity-increasing effect is shown during thyroid imaging of a mouse (Fig. 5); since the tiny mouse thyroid fits into a square millimetre, it can be placed at half a centimetre from the

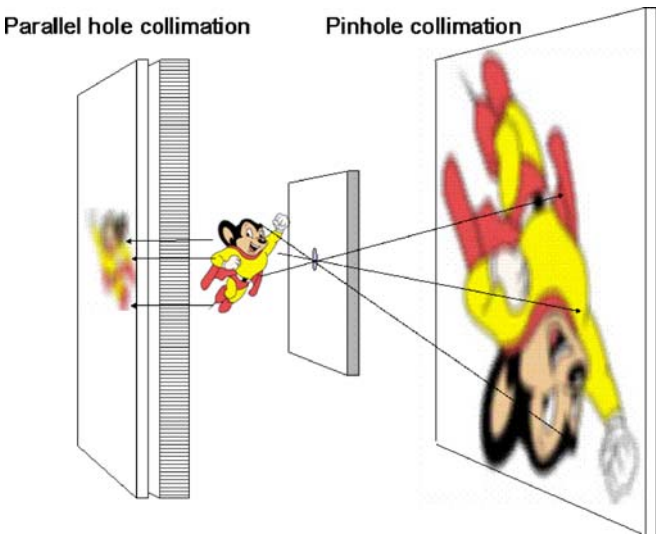

Fig. 3. With parallel-hole collimation (*left*), image resolution can be degraded significantly owing to intrinsic camera blurring. With pinhole imaging (*right side of the mouse*), magnification of the projection suppresses information loss due to intrinsic camera blurring

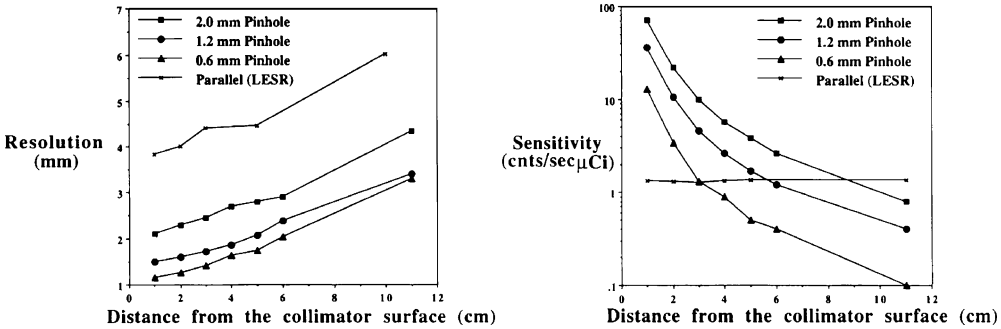

Fig. 4. Advantages of a pinhole system over parallel-hole collimation. When an object is imaged from a short distance, a better image resolution can be obtained, and at the same time the detected fraction of photons (sensitivity) can be much higher (source: R.J. Jaszczak et al. [19], with permission of *Physics in Medicine and Biology*)

pinhole. As a result, a magnification factor of more than 20 can be obtained. Despite the fact that R_i of the camera was 3.1 mm for this particular example, details of approximately 150 μm could still be visualised.

The resolution of a pinhole system for an "ideal" detector (with R_i=0) is roughly described in Eq. 1, and is also called the geometric resolution R_g of the pinhole device:

$$R_g \approx D(l+z)/l \tag{1}$$

Here, l is the distance between the pinhole and the detector. This equation shows that the pinhole diameter dramatically affects the resolution, particularly when pinhole-to-object distance increases. The effects of a limited detector resolution are taken into account in Eq. 2. Here the total system resolution R_t is approximated by:

$$R_t \approx \sqrt{\left[\left(\frac{z}{l}R_i\right)^2 + R_g^2\right]} \tag{2}$$

Equation 2 shows that limited intrinsic resolution can degrade the total system resolution dramatically. Note that penetration of rays along the pinhole edge can be accounted for by using effective diameters rather than physical diameters. Accurate mathematical descriptions of effective hole diameters, in terms of resolution and sensitivity, can be found in [21] and [22].

Pinhole SPECT devices and image reconstruction

With the development of advanced algorithms that are currently available to reconstruct images from complex pinhole geometries, images of superior resolution and quantitative accuracy can be produced. Consequently almost all dedicated small animal SPECT systems are presently fitted with pinholes. Usually one rotates either the animal or the detectors with collimators to acquire a sufficient number of angular views ("projections") to enable reconstruction of 3D volume images. SPECT systems can be fitted with one [e.g. 23–25], two [e.g. 26], three [e.g. 19, 27], four [28], six [e.g. 29] or even more pinholes. In some cases the use of many pinholes will produce overlapping projections (often referred to as multiplexed projections) [30, 31]. In addition to rotation-based systems, there are stationary systems: these often have many pinholes and are able to deliver excellent spatial and temporal resolution. Two types of stationary system with many non-overlapping projections will be discussed in a following section.

The issue of overlapping versus non-overlapping projections is the subject of many scientific discussions and ongoing research. Overlap increases system sensitivity but one has to keep in mind that this increase is at least partly artificial, since a significant amount of information per photon can be lost owing to the overlap. Therefore, the sensitivity of systems based on overlapping projections cannot be compared with that of systems with non-overlapping projections. The comparison is complicated since information loss owing to overlap strongly depends on the

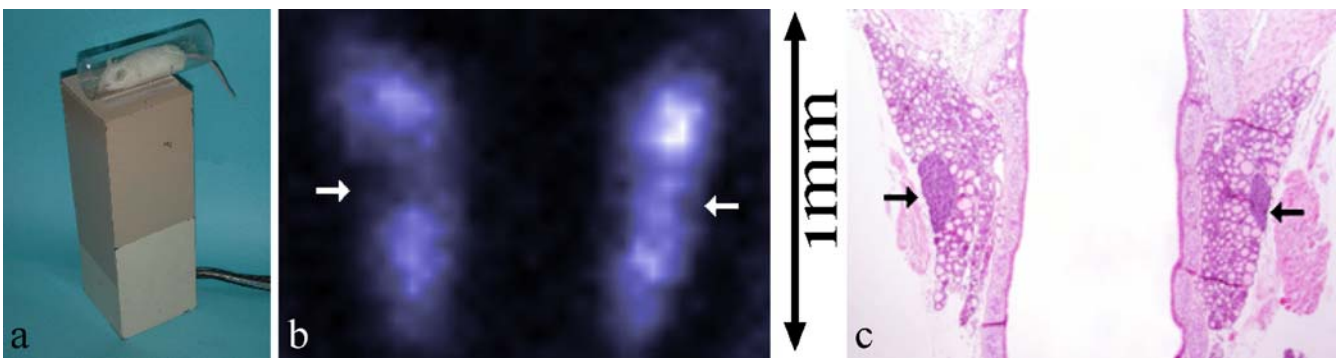

Fig. 5. a Desktop mouse pinhole imaging system. **b** ^{125}I scan of a mouse thyroid (size ≈1×1 mm) provides details of a few hundred micrometres, such as the parathyroid gland, which does not take up any iodine (*arrows*, also shown in frame **c**). (From [20])

distribution that is imaged. For example, the image degradation gets stronger with higher background activity and with extended tracer distributions. The latter are much more common than distributions of tracers that accumulate in small areas. In some cases overlapping projections can be used to increase the field of view. In addition, allowing overlap is a way to increase the number of viewing angles of a volume of interest. Research on the extent, if any, to which overlap is beneficial for specific tasks and distributions is ongoing in several imaging laboratories.

In principle, image reconstruction from pinhole SPECT projection images can be performed analytically, using filtered back projection-like algorithms (e.g. the Feldkamp algorithm [32]). These algorithms are also used in other cone-like radiation-transport geometries such as X-ray CT systems and cone-beam collimated SPECT systems (cone-beam collimators, just like parallel-hole collimators, have long holes but these holes are directed to a focal point). The advantage of these analytical methods is their computational speed, but (a) they have limited robustness to quantum noise that is present in projections, (b) they do not compensate for image blurring effects and (c) they are not really flexible enough to handle the complicated pinhole and detector placements needed to extract the maximum amount of information from the object being imaged. Therefore, at present, with most pinhole systems iterative methods of reconstruction are used, such as the maximum likelihood expectation maximisation (ML-EM [33]). The ML-EM algorithm is a statistical algorithm which takes into account the characteristics of the noise in gamma camera pixels. In addition, these algorithms can incorporate models of image degradation such as non-uniformities and distance-dependent sensitivity. Other factors, such as spatial variant resolution and radiation penetration along the pinhole edges, can also be included [30, 34, 35] in order to correct for these image-degrading effects. As a result, statistical algorithms produce images with less noise, better resolution and higher quantitative accuracy than many other algorithms.

A simple explanation of image reconstruction

Although sometimes complicated to implement in a real pinhole system, the basics of iterative reconstruction can be explained quite simply to those who remember simple high school algebra. The task in iterative reconstruction in emission tomography is to attempt to solve a linear set of hundreds of thousands of equations with typically hundreds of thousands of unknowns. Such a set of equations is shown in Fig. 6a: the unknown numbers A_i (together forming a so-called vector **A**, with element indexes i ranging from 1 to V) are the amounts of radioactive tracer present in each tiny volume element (voxel) within the object. The process of "iterative reconstruction" involves the repeated application of a set of operations that progressively gets closer to a correct estimate of the unknown activity distribution. Figure 6b shows the concept of this iterative updating. At the end of a reconstruction, each of the estimated numbers can be transformed to colour- or grey-scale pixels for visualisation.

Before the iterative calculations can start, one needs a set of numbers (matrix elements) in which each of the elements M_{ji} represents a probability that gamma quanta emitted by an amount of tracer A_i present in a voxel i will be detected in a pixel j at one of the detectors. These elements need to be known for each individual voxel–pixel combination. The entire set of measured projection pixels is represented by a vector **P**. The numbers M_{ji} together with **P** determine the set of equations from which the activity distribution **A** has to be solved. For example, during an iteration of the ML-EM algorithm, the actual estimate of **A** (which we call $\mathbf{A}^e$) is used to generate an estimate of the projection, denoted with vector $\mathbf{P}^e$, simply by carrying out the summations, as presented in Fig. 6a, but with $\mathbf{A}^e$ instead of **A**. Next, ML-EM uses the relative differences between **P** and $\mathbf{P}^e$, to calculate an object error map. The error map is used to update $\mathbf{A}^e$ with a simple equation. The basic idea behind all iterative methods is that when $\mathbf{P}^e$ is very close to **P**, $\mathbf{A}^e$ must be close to the reality **A**, because it produces almost the same projection as does **A**. The generation of a new $\mathbf{P}^e$ and the updating of $\mathbf{A}^e$ often need to be repeated hundreds of times to obtain a good solution. Because of the

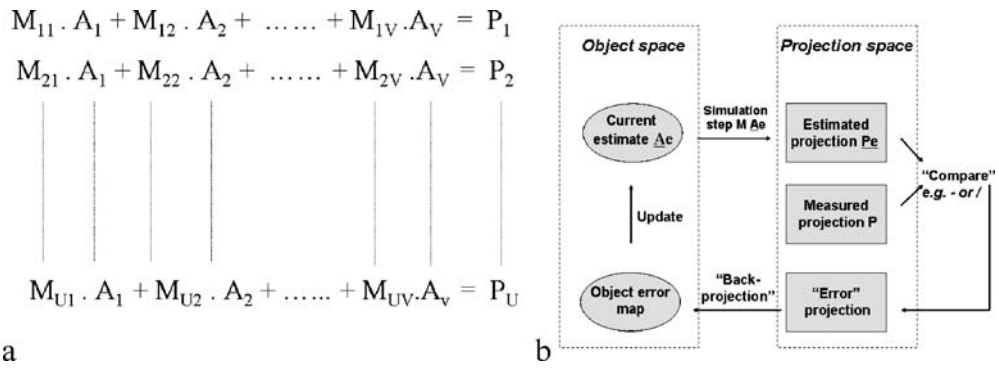

Fig. 6. a Set of linear equations describing how activity in the object is mapped onto the projection images. This set is used in iterative methods to obtain the reconstructed volume image (with a total of V different elements of vector **A**) from the pinhole camera projection pixel contents P with a total of U pixels. U and V are numbers in the order of a couple of hundreds of thousands. The iterative scheme is shown in **b**

many iterations required, acceleration methods to speed up the algorithms have been developed. The ordered subset expectation maximisation (OS-EM, [36]) is currently the most popular method.

Simple introductions to the subject of iterative SPECT image reconstruction, and information on how to carry out comparisons and update steps during reconstruction, can be found in [37, 38]. The accurate determination of the matrix elements in M is difficult, often requiring complex calculations and/or measurements that are specific to each different pinhole SPECT device. An accurate match of the matrix elements and real detection probabilities has a critically important influence on the reconstructed image; the number of iterations and quality of image smoothing for noise suppression are also important.

Stationary SPECT systems

Some pinhole systems require rotation of either the detector or the animal, while others are stationary pinhole systems. Early clinical stationary pinhole systems were developed in the early 1970s by Wouters et al. [11], Chang et al. [12] and Vogel et al. [18]. The systems in [11] and [18] were based on only seven pinholes. Various shapes of apertures other than pinholes, some of which were time coded, were also investigated at that time (see [39]). Later, several papers about exciting stationary pinhole SPECT system designs were published by the University of Arizona [e.g. 40]. In addition, a modular stationary SPECT device was tested and presented in 1993 [41]. Later, systems with 24 pinholes (FastSPECT I) and 16 pinholes (FastSPECT II) were constructed [e.g. 42, 43]. Resolutions better than 2 mm were already reported in 1998 with FastSPECT [44]. As resolution improved over the years, FastSPECT produced impressive myocardial images of rats [45] and was also used for other biological studies.

An advantage of stationary SPECT systems is that they can perform arbitrarily short data acquisitions that contain all the viewing angles required to reconstruct a tomographic image, which is similar to the situation in most PET systems. Because of the high number of pinholes, which provide a high sensitivity, stationary systems are ideal for dynamic imaging and assessing tracer and pharmaceutical kinetics. In addition, these stationary systems are inherently very stable over time.

In 2004 the University Medical Centre, Utrecht, completed the construction of a stationary ultra-high-resolution system (U-SPECT-I [35]). A tube with 75 focussed gold pinholes was put inside a set of three detectors borrowed from a clinical system. A robot was used for calibration and for total body imaging protocols. An improved stand-alone version ("U-SPECT-II", Fig. 7) was recently launched based on three large field of view detectors that allow for an even better sensitivity and resolution than U-SPECT-I. Prototypes of future U-SPECT devices with CCD-based detectors are currently under development (e.g. the U-SPECT-III [46]). In all U-SPECT systems, the animal is surrounded by many pinholes placed

Fig. 7. The U-SPECT-II system based on ultra-large NaI detectors and interchangeable collimator tubes

in rings. This large set of pinholes allows us to obtain a sufficient number of different angular views for reconstruction of cross-sectional images of the object, without having to change the position of the detectors, the pinholes or the animal. We used U-SPECT-I to scan the first living animals in the spring of 2004, and immediately obtained images with sub-millimetre resolution: 0.45 mm along all axes could be achieved with 0.6-mm pinholes, and currently, with pinholes of 0.3 mm, a resolution of 0.35 mm (0.04 μl) has been achieved [35, 47], Fig. 8). U-SPECT-I is equipped with a large number of pinholes, namely 75, and also differs in several other respects from FastSPECT: in U-SPECT the pinholes are much more focussed as a result of a novel two-stage collimation method that prevents projection overlap and allows for close packing of projections on the detector surface. Furthermore, the geometry chosen uses three large detectors and results in a high magnification factor which helps to improve resolution. Instead of using relatively expensive modular gamma cameras that contain a large amount of dead area at the edges, our system creates separated but closely packed projections on large-area detectors. The large number of independent pinhole cameras created in this way facilitates the detection of a large number of gamma quanta from the volume that one really wants to scan (e.g. the heart or brain); as a result, hardly any detector area is wasted by projecting irrelevant parts of the animal. We have also found that it is very easy to image large volumes with U-SPECT, up to entire animals. For example, using the same focussing collimator we were able to obtain total body scans of mice at approx. 0.5-mm resolution [48]. To this end the bed can be shifted

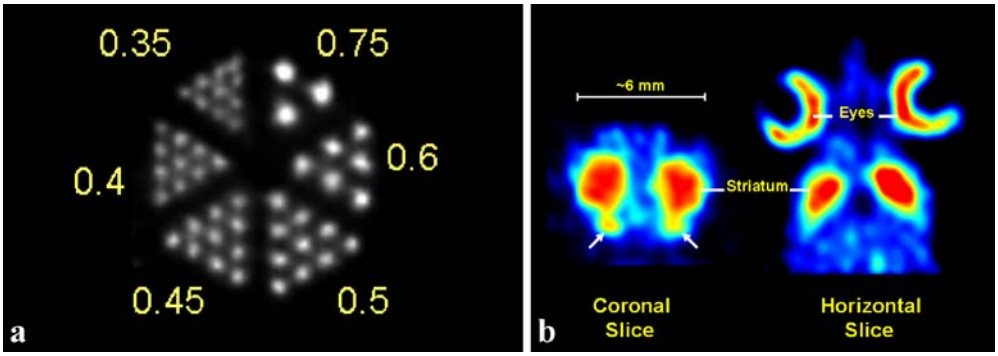

Fig. 8. U-SPECT images. **a** Derenzo resolution phantom image obtained with U-SPECT (0.3-mm pinholes) shows a section with 0.35-mm capillaries clearly separated. **b** Two mutual perpendicular cross-sections of a 3D sub-millimetre resolution FP-CIT image of the distribution of dopamine transporters in a mouse head obtained with U-SPECT-I fitted with 0.6-mm pinholes. Dynamics of tracer concentrations in tiny structures in sub-compartments of mouse organs such as the olfactory tubercle (arrows) and the retina can be monitored

in x, y and z direction, in order to acquire gamma radiation from an arbitrarily large part of the animal.

Further improvement of small animal SPECT instruments

There are several ways to improve imaging characteristics of small animal SPECT devices. These include the development of better algorithms and software for image reconstruction, optimised collimators and better detectors. Some systems are already equipped with close to optimal image reconstruction methods which perform accurate resolution recovery and which result in good quantitative accuracy. In these systems the match between the calculated/measured reconstruction matrix elements and the physical detection likelihoods has to be very accurate and sufficiently stable over time. Therefore, one needs very good system calibration which can be carried out with point source measurements. Much important information about pinhole SPECT reconstruction and the associated estimation of the matrix elements has already been published [e.g. 21, 35, 47, 49–52].

Mathematical investigations are in progress to improve pinhole system geometries [e.g. 53, 54]. These investigations can be highly complex owing to the many degrees of freedom in system geometry. Candidates for future systems include systems that have a huge number of tiny pinholes; in some designs, pinholes have a diameter of close to zero, and therefore transmission of gamma quanta is mainly based on material penetration effects [53].

The position-sensitive gamma ray detector of a SPECT pinhole camera module is in many respects like the retina of the eye since, for example, its quality strongly influences overall system performance. If possible, the detector should have such a high resolution that the system resolution is not markedly affected by detector blur, but this is not the case yet for any commercial pinhole SPECT system. So far, high-resolution detectors have been used only in mini-scale toy systems. The development of affordable high-resolution radiation detectors is very important to improve SPECT systems, and also for other biomedical applications. Many successful attempts have been made to manufacture high-resolution detectors [e.g. 55–66]. However, these are almost all at the prototype stage, to some extent owing to the high costs of obtaining a surface area large enough to serve a large number of pinholes. Efforts are being made to simulate and construct compact high-resolution systems based on CCDs or other detectors [41, 46, 49, 67–70].

For gamma quanta that travel along exactly the same line towards the detector, interaction can take place at different depths in the detector material (e.g. the scintillation crystal). Gamma detectors as currently in use for pinhole SPECT will attribute these gamma rays to a different ray direction, which will result in parallax errors and therefore in a blurred reconstruction. This is called the depth-of-interaction (DOI) problem. An ideal gamma camera should have high resolution not only for radiation that enters the detector from a direction perpendicular to the detector surface but also for gamma rays that enter the crystal at any angle. So ideally a ray entering a crystal at a certain point and at a certain angle should always provide the same 2D coordinate, independent of the depth at which the interaction in the crystal occurred. One way to achieve this is to use a thin crystal, but then only a small fraction of gamma quanta can be detected. Another method is to use a curved detector surface like those present in biological systems, but these can be hard to produce. With scintillation detectors it is also possible to use optical techniques to avoid the DOI problem (e.g. [46, 49, 71]), or to use depth encoding methods in order to derive the exact point at which the gamma ray entered the crystal surface. Also, direct conversion detectors (which are not based on scintillation but convert gamma rays directly into an electrical signal) have been proposed that allow DOI to be corrected by using a 3D read out [57].

As an alternative to pinholes, collimators based on slits have been proposed for small animal SPECT. Some have a single-stage slit collimation [72] followed by collimation with a stack of slats. A drawback of such a slit collimation is that magnification effect, which has been shown to be

very beneficial to pinhole imaging, is only present in the transaxial direction, which leads to a poor image resolution in the axial direction. The slats effectively result in parallel-hole collimation, including its associated blurring effects in the axial direction. As an alternative, Huang and Zeng from Utah recently proposed two-stage slit collimation with crossed slits, where each crossing of two perpendicular slits forms a kind of generalised pinhole collimator [73]. The system with crossed slits can have adjustable sensitivity and independent magnification factors in different directions, and could form the basis of a flexible high-resolution system.

Collimators only allow the detection of photons that have travelled in narrowly selected directions towards the detector, and therefore only a small fraction of all gamma rays can be used with collimated systems. This is a major drawback of SPECT compared with PET. If SPECT evolves along similar directions as eyes have evolved, pinholes will no longer be required. Indeed, some developments are directed towards the replacement of collimators. For example, lens-based systems [e.g.,74, 75] and gamma ray mirrors [76–78] have been proposed. However, it remains to be seen whether gamma lens or gamma mirror-based gamma cameras will ever be able to compete with collimation-based systems, because there are many complications. For example, the space required for a gamma lens is currently of the order of several metres [75], which will be generally too large for practical purposes. An overview of alternatives to collimators is given in [34].

Some applications of ultra-high-resolution SPECT

Major tools for unravelling the function of genes and identifying physiological and patho-physiological mechanisms underlying diseases currently include mouse models and a variety of evaluation methods, including histological/biochemical techniques. Standard histology, immuno-protein staining, in situ hybridisation and autoradiography techniques can all be used to show the spatial distribution of tissue, cells, proteins or mRNA. However, these methods are extremely laborious and carry the methodological risk associated with working ex vivo. As a result, the current practice of phenotyping mouse strains is quite limited. In addition, there is a strong societal pressure to refine first-line screening of experimental drugs, thereby reducing animal discomfort and the required number of animals used. High-resolution animal SPECT will be a good alternative for part of this work, particularly when these systems become more affordable. SPECT and other molecular imaging devices are causing a revolution in fast functional analysis of mouse models since they enable one to look inside a living animal, and facilitate dynamic and follow-up studies. Moreover, a tremendous acceleration and refinement in the testing of experimental drugs can be expected. SPECT may also become more and more important as a pre-selection tool for timing of ex vivo methods such as autoradiography. In addition, the dynamic capabilities of new SPECT devices indicate that dynamic and kinetic pharmacologic studies may become an important new area of application of SPECT. Furthermore, tools are under development that will enable us to perform emission tomography on freely moving animals instead of anaesthetised animals [e.g. 79]. This will provide unique and new opportunities, particularly with regard to the study of brain function, and will facilitate continuous monitoring of molecule distributions in vivo.

High-resolution pinhole SPECT for clinical imaging

The recent introduction of ultra-high-resolution pinhole SPECT systems for animals has raised the question of whether it may soon be possible to develop very high resolution clinical pinhole systems for important areas of application such as heart or brain imaging. As mentioned in the course of this paper, pinholes have been used for clinical radionuclide imaging for many years, including the imaging of small organs like the thyroid, but they are still used in only a small fraction of all SPECT procedures. So far it seems that the advantages of pinholes are smaller when large body areas have to be imaged and when one is confined to scintillation gamma cameras with 3- to 4-mm intrinsic resolution. On the other hand, if one can focus enough pinholes on the organ of interest, the distance-related sensitivity drop that hampers non-focussing pinhole designs can be prevented. In addition, a stationary pinhole set-up can be created with focussing pinholes, which can be advantageous for dynamic cardiac imaging. Figure 9 shows

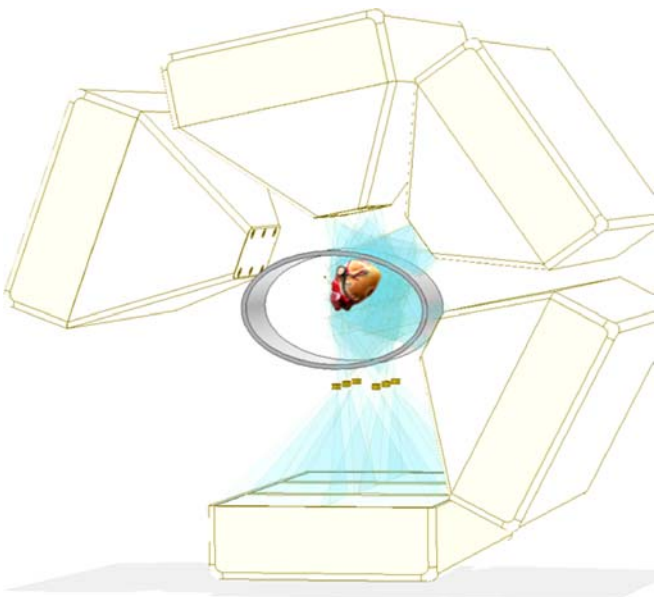

Fig. 9. Cardiac SPECT system model with pinholes focussing to the heart. In the picture the shielding was removed from one multi-pinhole collimator to show how the heart is projected onto the detector without overlap. Means to avoid projection overlap (baffles) are not shown. This system has a significantly better resolution–sensitivity trade-off than a dual-head parallel-hole SPECT system

an artist's impression of a focussing cardiac pinhole "toy model" that will be analysed below. This C-shaped detector set-up consists of five large detector blocks that each consist of three standard gamma cameras (R_i=3 mm, size 46×27 cm) with a radius of about 0.4 m and with a total of effectively 30 independent sub-detectors. The required field of view to project a large heart is assumed to be approx. 18 cm×15 cm when the pinhole magnification is set to 1.5, which corresponds to two projections per camera. With this system set-up in mind we now can complete some rough calculations to compare standard clinical SPECT with this pinhole system:

The sensitivity of a dual-head parallel-hole SPECT system (ParHole system) , with low-energy high-resolution (LEHR, hole diameter 1.4 mm and hole length 33 mm) parallel-hole collimators, is about 146 cpm/μCi per detector head, which is equivalent to a total geometric sensitivity of 0.017%. In the centre of the heart a resolution of about 8.7 mm is reached at 15.5 cm, which is assumed to be the average distance between the collimator and the centre of the left ventricle in the comparison we do here between a stationary pinhole and the ParHole system. In order to achieve an equal system resolution at 15.5 cm with a pinhole camera, the pinhole diameter needs to be 4.9 mm, corresponding to a sensitivity of approx. 0.006%. The pinhole set-up in Fig. 9, with 30 independent pinhole cameras, has a sensitivity of 0.15%, which is almost one order of magnitude higher than the sensitivity of the ParHole system. This indicates that one can make a scan with approximately the same resolution but almost ten times faster than with a ParHole system. Alternatively, one can reduce the pinhole diameter to increase resolution. When we choose 1.63 mm, the efficiency is decreased to 0.017%, which is equal to the ParHole system. However, now the pinhole system has a 2.1 times higher system resolution than the ParHole system (4.1 mm instead of 8.7 mm). If, in addition, the intrinsic resolution of the detectors were to be 1.0 mm instead of 3.0 mm, it would be possible to achieve a system resolution better than 3 mm. This could mean an improvement over clinical PET systems. Note that the improvements over ParHole SPECT calculated here are based on projecting a large heart without projection overlap. With normal hearts, significantly larger improvements can be obtained since more focussing pinholes can be used. Then, however, a strategy is required to extend the field of view for imaging larger hearts. Finally, when large detector areas are available for the construction of clinical SPECT systems, pinholes will not be the only gateway to significantly improved performance: other focussing collimators (cone beam, multiple parallel-hole collimators, crossed slits, slit-slat collimators, rotating mini-cameras etc,) will certainly be worth considering, too.

Concluding remarks

Pinhole collimated imaging systems have been around for millions of years, for example in primitive eyes. Although collimation is inherently inefficient, its basic principles have been very useful for the construction of SPECT devices. The many kinds of eyes that have evolved from pinhole eyes [80] can be a source of inspiration to engineers in searching for alternatives to traditional gamma ray collimators and the currently used sub-optimal gamma ray detectors.

In recent years, significant progress has been made with the construction of small animal SPECT imaging. Even if developments are initially confined to the straightforward evolution of proven and readily available building blocks in concert with pinhole-like collimators, significant further improvements in both preclinical and clinical SPECT instruments can be expected. To further improve SPECT devices we need to direct our efforts to the production of low-cost high-resolution radiation detectors. Many other interesting developments are ongoing in SPECT system engineering. The many new and unforeseen applications that will spin off from high-resolution and flexible SPECT technology, together with new tracers and biological models, are expected to contribute to a revolution in biomedical research.

Acknowledgements. The authors thank Dr. Cynthia Jongen, Dr. Steven Staelens, Dr. Mart Rentmeester, Dr. Wojtek Zbijewski, Dr. Julia Huijbregts, Dr. Jeroen Pasterkamp, Brendan Vastenhouw (University Medical Centre Utrecht) and Prof. Brian Hutton (University College London) for many constructive comments. Dr. Freek Beekman is a board member and share holder of Molecular Imaging Laboratories, The Netherlands.

References

1. King MA, Pretorius PH, Farncombe T, Beekman FJ. Introduction to the physics of molecular imaging with radioactive tracers in small animals. J Cell Biochem Suppl 2002;39:221–30.
2. Meikle SR, Kench P, Kassiou M, Banati RB. Small animal SPECT and its place in the matrix of molecular imaging technologies. Phys Med Biol 2005;50(22):R45–61.
3. Meikle SR, Beekman FJ, Rose SE. Complementary molecular imaging technologies: high resolution SPECT, PET and MRI (invited review). Drug Discov Today Technol 2006;3(2):187–94
4. Land MF. The spatial resolution of the pinhole eyes of giant clams (*Tridacna maxima*). Proc Biol Sci 2003;270(1511):185–8.
5. Hammond JH. The camera obscura, a chronicle. Bristol: Adam Hilger Ltd; 1981.
6. Marignier JL. Historical light on photography. Nature 1990; 346:115.
7. Copeland DE, Benjamin EW. Pinhole camera for gamma-ray sources. Nucleonics 1949;5:45–9.
8. Anger HO. Scintillation camera. Rev Sci Instr 1958;29:27–33.
9. Mallard JR, Myers MJ. The performance of a gamma camera for the visualization of radioactive isotopes in vivo. Phys Med Biol 1963;8:165–82.
10. Wanet PM, Sand A, Abramovici J. Physical and clinical evaluation of high-resolution thyroid pinhole tomography. J Nucl Med 1996;37:2017–20.
11. Wouters A, Simon KM, Hirschberg JG. Direct method of decoding multiple images. Appl Opt 1973;12:1871.

12. Chang LT, Kaplan SN, Macdonald B, Perez-Mendez V, Shiraishi L. A method of tomographic imaging using a multiple pinhole coded aperture. J Nucl Med 1974;15:1063–5.
13. Seret A, Defrise M, Blocklet D. 180° Pinhole SPET with a tilted detector and OS-EM reconstruction: phantom studies and potential clinical applications. Eur J Nucl Med Mol Imaging 2001;28(12):1836–41.
14. Seret A, Flérès D, Firket O, Defrise M. Body contour 180° pinhole SPET with or without tilted detector: a phantom study. Eur J Nucl Med Mol Imaging 2003;30(9):1205–10.
15. Maillefert JF, Toubeau M, Piroth C, Piroth L, Brunotte F, Tavernier C. Bone scintigraphy equipped with a pinhole collimator for diagnosis of avascular necrosis of the femoral head. Clin Rheumatol 1997;16(4):372–7.
16. Pak Y-H, Bahk Y-W. Combined scintigraphic and radiographic diagnosis of bone and joint diseases. Berlin Heidelberg New York: Springer; 2004.
17. Spanu A, Falchi A, Manca A, Marongiu P, Cossu A, Pisu N, et al. The usefulness of neck pinhole SPECT as a complementary tool to planar scintigraphy in primary and secondary hyperparathyroidism. J Nucl Med 2004;45(1):40–8.
18. Vogel RA, Kirch D, LeFree M, Steele P. A new method of multiplanar emission tomography using a seven pinhole collimator and an Anger scintillation camera. J Nucl Med 1978;19: 648–54.
19. Jaszczak RJ, Li J, Wang H, Zalutsky MR, Coleman RE. Pinhole collimation for ultra-high-resolution small-field-of-view SPECT. Phys Med Biol 1994;39:425–37.
20. Beekman FJ, McElroy DP, Berger F, Gambhir SS, Hoffman EJ, Cherry SR. Towards in vivo nuclear microscopy: I-125 imaging in mice using micro-pinholes. Eur J Nucl Med Mol Imaging 2002;29(7):933–8.
21. Metzler SD, Bowsher JE, Greer KL, Jaszczak RJ. Analytic determination of the pinhole collimator's point-spread function and RMS resolution with penetration. IEEE Trans Med Imaging 2002;21(8):878–87.
22. Accorsi R, Metzler SD. Analytic determination of the resolution-equivalent effective diameter of a pinhole collimator. IEEE Trans Med Imaging 2004;23(6):750–63.
23. Palmer J, Wollmer P. Pinhole emission computed tomography: method and experimental evaluation. Phys Med Biol 1990;35: 339–50.
24. Habraken JBA, de Bruin K, Shehata M, Booij J, Bennink R, van Eck Smit BL, et al. Evaluation of high-resolution pinhole SPECT using a small rotating animal. J Nucl Med 2001;42: 1863–9.
25. Wu MC, Tang HR, Gao DW, Ido A, O'Connell JW, Hasegawa BH, et al. ECG gated pinhole SPECT in mice with millimeter resolution. IEEE Trans Nucl Sci 2000;47:1218–27.
26. McElroy DP, MacDonald LR, Beekman FJ, Wang YC, Patt BE, Iwanczyk JS, et al. Performance evaluation of A-SPECT: a high resolution desktop pinhole SPECT system for imaging small animals. IEEE Trans Nucl Sci 2002;49:2139–47.
27. Acton PD, Choi SR, Plossl K, Kung HF. Quantification of dopamine transporters in the mouse brain using ultra-high resolution single-photon emission tomography. Eur J Nucl Med Mol Imaging 2002;29:691–9.
28. Ishizu K, Mukai T, Yonekura Y, Pagani M, Fujita T, Magata Y, et al. Ultra-high-resolution SPECT system using four pinhole collimators for small animal studies. J Nucl Med 1995;26: 2282–9.
29. Moore SC, Zimmerman RE, Mahmood A, Mellen R, Lim CB. A triple-detector multi-pinhole system for SPECT imaging of rodents. J Nucl Med 2005;45(5):97P.
30. Schramm NU, Ebel G, Engeland U, Schurrat T, Béhé M, Behr TM. High-resolution SPECT using multipinhole collimation. IEEE Trans Nucl Sci 2003;50(3):315–20.
31. Meikle SR, Fulton RR, Eberl S, Dahlbom M, Wong KP, Fulham MJ. An investigation of coded aperture imaging for small animal SPECT. IEEE Trans Nucl Sci 2001;48:816–21.
32. Feldkamp LA, Davis LC, Kress JW. Practical cone-beam algorithm. J Opt Soc Am 1984;A1:612–9.
33. Lange K, Carson REM. Reconstruction algorithms for emission and transmission tomography. J Comput Assist Tomogr 1984;8: 306–16.
34. Furenlid LR, Chen Y, Kim H. SPECT imager design and data acquisition systems. In: Kupinski MA, Barrett HH, editors. Small animal SPECT imaging. New York: Springer Science+ Business Media Inc.; 2005, p.115–38.
35. Beekman FJ, van der Have F, Vastenhouw B, van der Linden AJA, van Rijk PP, Burbach JPH, et al. U-SPECT-I: a novel system for sub-millimeter resolution tomography of radiolabeled molecules in mice. J Nucl Med 2005;46:1194–200.
36. Hudson HM, Larkin RS. Accelerated image reconstruction using ordered subsets of projection data. IEEE Trans Med Imaging 1994;13:601–9.
37. Hutton BF, Hudson HM, Beekman FJ. A clinical perspective of accelerated statistical reconstruction. Eur J Nucl Med 1997;24: 797–808.
38. Lalush DS, Wernick MN. Iterative Image reconstruction. In: Wernick MN, Aarsvold JN, editors. Emission tomography: the fundamentals of PET and SPECT. San Diego: Academic Press; 2004.
39. Barrett HH, Swindell W. Radiological imaging. The theory of image formation, detection, and processing. New York: Academic Press; 1981.
40. Rogulski MM, Barber HB, Barrett HH, Shoemaker RL, Woolfenden JM. Ultra-high-resolution brain SPECT: simulation results. IEEE Trans Nucl Sci 1993;40:1123–9.
41. Rowe RK, Aarsvold JN, Barrett HH, Chen JC, Klein WP, Moore BA, et al. A stationary hemispherical SPECT imager for three-dimensional brain imaging. J Nucl Med 1993;34:474–80.
42. Patton DD, Barrett HH, Chen JC, Klein WP, Pang I, Richards D, et al. FASTSPECT—a 4-dimensional brain imager. J Nucl Med 1994;35(5):P93, Suppl S.
43. Furenlid LR, Wilson DW, Chen Y, Kim H, Pietrski PJ, Crawford MJ, et al. FastSPECT II: a second-generation high-resolution dynamic SPECT imager. IEEE Trans Nucl Sci 2004;51:631–5.
44. Kastis GK, Barber HB, Barrett HH, Gifford HC, Pang IW, Patton DD, et al. High resolution SPECT imager for three-dimensional imaging of small animals [abstract]. J Nucl Med 1998;39(5):25 Suppl S 9P.
45. Liu Z, Kastis GA, Stevenson GD, Barrett HH, Furenlid LR, Kupinski MA, et al. Quantitative analysis of acute myocardial infarct in rat hearts with ischemia-reperfusion using a high-resolution stationary SPECT system. J Nucl Med 2002;43 (7):933–9.
46. Beekman FJ, Vastenhouw B. Design and simulation of a high-resolution stationary SPECT system for small animals. Phys Med Biol 2004;49:4579–92.
47. van der Have F, Vastenhouw B, Rentmeester MCM, Beekman FJ. System calibration and statistical image reconstruction for sub-mm stationary pinhole SPECT. Conference record of the 2005 Nuclear Science Symposium and Medical Imaging Conference, Puerto Rico, M11-291, 2005.
48. Vastenhouw B, Beekman FJ. Sub-mm total body mouse imaging with U-SPECT-I. J Nucl Med 2007 (in press).

49. Kupinski MA, Barrett HH, editors. Small-animal SPECT imaging. New York: Springer Science+Business Media Inc., 2005.
50. Zeniya T, Watabe H, Aoi T, Kyeong MK, Teramoto N, Hayashi T, et al. A new reconstruction strategy for image improvement in pinhole SPECT. Eur J Nucl Med Mol Imaging 2004;31 (8):1166–72.
51. Beque D, Nuyts J, Suetens P, Bormans G. IEEE Trans Med Imaging 2003;22(5):599–612.
52. Metzler SD, Greer KL, Jaszczak RJ. Determination of mechanical and electronic shifts for pinhole SPECT using a single point source. IEEE Trans Med Imaging 2005;24(3):361–70.
53. Rentmeester MCM, van der Have F, Beekman FJ. Continuous model of multi-pinhole SPECT devices. Conference Record of the 2005 IEEE Nuclear Science Symposium and Medical Imaging Conference, Puerto Rico. IEEE 2005;M03–283.
54. Cao ZX, Bal G, Accorsi R, Acton PD. Optimal number of pinholes in multi-pinhole SPECT for mouse brain imaging—a simulation study. Phys Med Biol 2005;50(19):4609–24.
55. Barber HB. Applications of semiconductor detectors to nuclear medicine. Nucl Instrum Methods Phys Res A 1999;436:102–10.
56. Fiorini C, Longoni A, Perotti F, Labanti C, Rossi E, Lechner P, et al. A monolithic array of silicon drift detectors coupled to a single scintillator for gamma-ray imaging with sub-millimeter position resolution. Nucl Instrum Methods Phys Res A 2003;512:265–71.
57. He Z, Li W, Knoll GF, Wehe DK, Berry J, Stahle CM. 3-D position sensitive CdZnTe gamma-ray spectrometers. Nucl Instrum Methods Phys Res A 1999;A422:173–8.
58. Lees JE, Fraser GW, Keay A, Bassford D, Ott R, Ryder W. The high resolution gamma imager (HRGI): a CCD based camera for medical imaging. Nucl Instrum Methods Phys Res A 2003;513(1–2):23–6.
59. Llopart X, Campbell M, Dinapoli R, Segundo DS, Pemigotti E. Medipix2: a 64-k pixel readout chip with 55-μm square elements working in single photon counting mode. IEEE Trans Nucl Sci 2002;49(5):2279–83.
60. Matherson KJ, Barber HB, Barrett HH, Eskin JD, Dereniak EL, Marks DG, et al. Progress in the development of larger-area modular 64×64 CdZnTe imaging arrays for nuclear medicine. IEEE Trans Nucl Sci 1998;45:354–8.
61. Miyaata E, Tamur K. Novel photon-counting detector for 0.1–100 keV X-ray imaging possessing high spatial resolution. Jpn J Appl Phys 2003;42:L1201–04, Part 2 No 10A.
62. Miyataa E, Mikia M, Tawaa N, Kamiyamaa D, Miyaguchi K. Development of new X-ray imaging device sensitive to 0.1–100 keV. Nucl Instrum Methods Phys Res A 2004;525:122–5.
63. Nagarkar VV, Shestakova I, Gaysinskiy V, Tipnis SV, Singh B, Barber W, et al. A CCD-based detector for SPECT. IEEE Trans Nucl Sci 2006;53(1):54–8.
64. Vavrik D, Jakubek J, Visschers J, Pospisil S, Ponchut C, Zemankova J. First tests of a Medipix-1 pixel detector for X-ray dynamic defectoscopy. Nucl Instrum Methods Phys Res A 2002;487(1–2):216–23.
65. de Vree GA, Westra AH, van der Have F, Moody I, Ligtvoet CM, Beekman FJ. Photon counting gamma camera based on an electron-multiplying CCD. IEEE Trans Nucl Sci 2005;52(3): 580–8.
66. Beekman FJ, de Vree GA. Photon-counting versus an integrating CCD-based gamma camera: important consequences for spatial resolution. Phys Med Biol 2005;50(12): N109–19.
67. Kim H, Furenlid LR, Crawford MJ, Wilson DW, Barber HB, Peterson TE, et al. SemiSPECT: a small-animal single-photon emission computed tomography (SPECT) imager based on eight cadmium zinc telluride (CZT) detector arrays. Med Phys 2006;33(2):465–74.
68. Kastis GA, Wu MC, Balzer SJ, Wilson DW, Furenlid LR, Stevenson G, et al. Tomographic small-animal imaging using a high-resolution semiconductor camera. IEEE Trans Nucl Sci 2002;49(1):172–5.
69. Meng LJ, Clinthorne NH, Skinner S, Hay RV, Gross M. Design and feasibility study of a single photon emission microscope system for small animal I-125 imaging. IEEE Trans Nucl Sci 2006; accepted for publication.
70. Funk T, Després P, Barber WC, Shah KS, Hasegawa BH. A multipinhole small animal SPECT system with submillimeter spatial resolution. Med Phys 2006;33(5):1259–67.
71. Beekman FJ. Stralingsdetectieinrichting. Dutch patent application, NL-1029558, July 2005.
72. Walrand S, Jamar F, de Jong M, Pauwels S. Evaluation of novel whole-body high-resolution rodent SPECT (Linoview) based on direct acquisition of linogram projections. J Nucl Med 2005;46(11):1872–80.
73. Huang Q, Zeng GL. An analytical algorithm for skew-slit imaging geometry with nonuniform attenuation correction. Med Phys 2006;33(4):997–1004.
74. Snigirev A, Kohn V, Snigireva I, Lengeler B. A compound refractive lens for focusing high-energy X-rays. Nature 1996;384: 49–51.
75. Pivovaroff MJ, Barber WB, Christensen FE, Craig WW, Decker T, Epstein M, et al. Small-animal radionuclide imaging with focusing gamma-ray optics. Proc SPIE Int Soc Opt Eng 2004;5199:147.
76. Serlemitsos PJ. Conical foil X-ray mirrors: performance and projections. Appl Opt 1988;27(8):1447–52.
77. Serlemitsos PJ, Soong Y. Foil X-ray mirrors. Astrophys Space Sci 1996;239:177–96.
78. Hildebrandt G, Bradazek H. Approaching real X-ray optics. The Rigaku Journal 2000;17:13–22.
79. Weisenberger AG, Gleason SS, Goddard J, Kross B, Majewski S, Meikle SR, et al. A restraint-free small animal SPECT imaging system with motion tracking. IEEE Trans Nucl Sci 2005;52(3):638–44.
80. Land MF. The optical structures of animal eyes. Curr Biol 2005;15(9):R319–23.